On the physical processes ruling an atmospheric pressure air glow discharge operating in an intermediate current regime

Cite as: Phys. Plasmas **22**, 023504 (2015); https://doi.org/10.1063/1.4907661
Submitted: 25 October 2014 • Accepted: 21 January 2015 • Published Online: 06 February 2015

L. Prevosto, H. Kelly, B. Mancinelli, et al.

On the physical processes ruling an atmospheric pressure air glow discharge operating in an intermediate current regime

L. Prevosto,[1,a)] H. Kelly,[1,2] B. Mancinelli,[1] J. C. Chamorro,[1] and E. Cejas[1]
[1]*Grupo de Descargas Eléctricas, Departamento Ing. Electromecánica, Facultad Regional Venado Tuerto (UTN), Laprida 651, Venado Tuerto (2600), Santa Fe, Argentina*
[2]*Instituto de Física del Plasma (CONICET), Facultad de Ciencias Exactas y Naturales (UBA) Ciudad Universitaria Pab. I, (1428), Buenos Aires, Argentina*

(Received 25 October 2014; accepted 21 January 2015; published online 6 February 2015)

Low-frequency (100 Hz), intermediate-current (50 to 200 mA) glow discharges were experimentally investigated in atmospheric pressure air between blunt copper electrodes. Voltage–current characteristics and images of the discharge for different inter-electrode distances are reported. A cathode-fall voltage close to 360 V and a current density at the cathode surface of about 11 A/cm^2, both independent of the discharge current, were found. The visible emissive structure of the discharge resembles to that of a typical low-pressure glow, thus suggesting a glow-like electric field distribution in the discharge. A kinetic model for the discharge ionization processes is also presented with the aim of identifying the main physical processes ruling the discharge behavior. The numerical results indicate the presence of a non-equilibrium plasma with rather high gas temperature (above 4000 K) leading to the production of components such as NO, O, and N which are usually absent in low-current glows. Hence, the ionization by electron-impact is replaced by associative ionization, which is independent of the reduced electric field. This leads to a negative current-voltage characteristic curve, in spite of the glow-like features of the discharge. On the other hand, several estimations show that the discharge seems to be stabilized by heat conduction; being thermally stable due to its reduced size. All the quoted results indicate that although this discharge regime might be considered to be close to an arc, it is still a glow discharge as demonstrated by its overall properties, supported also by the presence of thermal non-equilibrium. © *2015 AIP Publishing LLC*. [http://dx.doi.org/10.1063/1.4907661]

I. INTRODUCTION

Typical sources for atmospheric pressure plasmas include arc, glow, corona, and dielectric barrier (DBD) discharges. In high-pressure arcs with currents > 1 A, the electron and gas temperatures usually exceed 6000 K in molecular gases.[1] Due to the high gas temperature, the dominant ionization mechanism is the thermal ionization, and the vibrational (T_{vib}) and rotational (T_{rot}) temperatures are almost equal to the kinetic (translational) temperature (T_g); being all of them close to the electron (T_e) temperature. Such kinds of plasmas are referred to as thermal or equilibrium plasmas[2] and are widely used for material processing (e.g., plasma cutting, spraying, etc).[3,4] On the contrary, glow, corona and DBD discharges typically produce non-equilibrium (cold plasmas) discharges with the gas temperature near room temperature $T_g \approx T_{rot} < T_{vib} < T_e$.[5–7] The non-equilibrium state is characterized by the presence of energetic electrons, that produce in turn ions and highly active chemical reactive species, but without the generation of excessive heat which could damage substrates. Owing to these features, cold plasmas have found widespread application in plasma biology and plasma medicine.[8–10]

The atmospheric pressure glow discharge has also attracted much attention in recent years as a promising source for non-equilibrium plasmas.[11–18] A large amount of these works have been conducted in low-current (~1 to 10 mA) regimes.[11,15,17,18] The normal low-pressure glow discharge is one of the most studied and widely applied non-equilibrium plasma discharge.[1] However, glow discharges at atmospheric pressure are hardly attainable due to instabilities which lead to a glow-to-arc transition.[1,19] As the pressure is increased the glow current density increases until reaching the threshold for the development of instabilities leading to a transition to the arc phase. There are at least two recognized mechanism resulting in glow to arc transition: (a) the contraction and thermalization of the discharge resulting from heating of the neutrals (the so called thermal instability[1]); and (b) heating of the cathode, resulting in the transition of secondary electron emission to thermionic emission of electrons from the cathode surface. In atomic gases, the main mechanism of energy transfer from the electrons to the gas is by elastic collisions. In molecular gases, however, electrons can transfer energy to additional molecular internal energy states, such as vibrational and rotational modes. Since the typical characteristic vibrational energy values (0.2–0.5 eV) are comparable to typical electron temperatures (of about 1 eV), most of the electron energy will be transferred to vibrational modes and partially to gas temperature through mechanisms of vibrational-translational relaxation.[6,7,15,17] As inelastic losses are usually greater than elastic ones by one to two orders of magnitude, molecular gases typically have higher heating rates and are more susceptible to

a)Electronic mail: prevosto@waycom.com.ar.

thermalization than atomic gases.[1,16] In a low-pressure glow, the thermal instabilities are usually suppressed by gas cooling at the boundaries. At atmospheric pressure, stable glow discharges are sometimes achieved by introducing a negative feedback between the discharge current and voltage. Large ballasted resistors[15] or high-impedance transformers[20] have been usually used to avoid the glow-to-arc transition.

Although the contraction of high-pressure glow discharges is often referred to as arcing, a stable (current limited) "hybrid" discharge lying between the strongly non-equilibrium plasma of a diffuse glow and the equilibrium plasma of a constricted arc can exists.[1] The temperatures T_e and T_g in an hybrid discharge differ appreciable, $T_e \approx 10\,000$ to $30\,000$ K, $T_g \approx 2000$ to 3000 K; but this difference is closer than that found in a low-pressure glow. The electron density can reach up to $10^{20}\,m^{-3}$ and the current density is greater than those found in the low-pressure glow but lower than the corresponding to an arc. Additionally, the electric field strength reaches an intermediate value between its characteristic values found in glow and arc discharges.[1]

This work describes an experimental characterization of a low-frequency, intermediate-current glow discharge operating in atmospheric pressure air between copper blunt electrodes for inter-electrode lengths from 0.1 to 11 mm and currents from 50 to 200 mA. A kinetic model for the ionization processes in the air discharge is also presented, with the aim of identifying the main physical processes ruling the discharge behavior. The results indicate the presence of a non-equilibrium plasma with rather high gas temperature (above 4000 K) thus causing that the ionization by electron-impact will be replaced with associative ionization. The paper is organized as follows: the experimental set-up is presented in Sec. II, while the experimental data are given in Sec. III. The kinetic model is described in Sec. IV, while the model results and its discussion are presented in Sec. V. The conclusions are summarized in Sec. VI.

II. EXPERIMENTAL SET-UP

A schematic of the circuit used to generate and analyze the atmospheric pressure low-current discharge is shown in Fig. 1. The electrodes (both 20 mm in diameter, with flat surfaces) were aligned vertically and supported in a variable gap electrode holder in free air. The anode was fixed in place, and the cathode (the lower grounded electrode) was moved using a micrometer to change the inter-electrode spacing d. The gap length was regulated between 0.1 and 11 mm with an uncertainty of about $\pm 50\,\mu$m. Commercial copper was used as the electrodes material. Several repeatable and consistent measurements were obtained after cleaning and re-polishing the electrode surfaces.

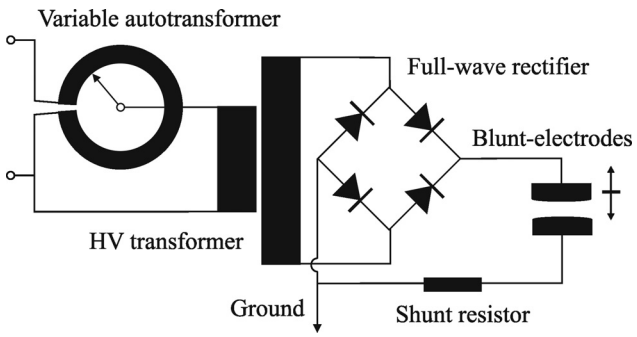

FIG. 1. Experimental set-up.

The ac power supply was a high-voltage transformer (25 kV, 100 mA, and 50 Hz) with a high-dispersion reactance (75 ± 0.5) kΩ connected to a variable autotransformer to control the discharge current. Since the high-impedance of the transformer provided an intrinsic current limitation, the use of external ballasts was not necessary. The output of the transformer was connected to a semiconductor full-wave rectifier to define the polarity of the electrodes. The discharge current was inferred from the measurement of the voltage drop across a shunt resistor (100 Ω) connected in series with the discharge, while the discharge voltage was measured by using a high-impedance voltage probe (Tektronix P6015A, 1000X, 3pf, 100 MΩ). Both electrical signals were simultaneously registered by using a 4-channel oscilloscope (Tektronix TDS 2004C with a sampling rate of 1 GS/s and an analogical bandwidth of 70 MHz).

Photographs of the plasma discharge were also taken using a charge-coupled device Lumenera digital camera with a spatial resolution of 640×480 pixels.

III. EXPERIMENTAL DATA

A. Current-voltage characteristic curves

Several voltage and current waveforms were taken for different electrode spacing. Typical signals of current (I) and voltage (V) for a 100 mA peak current and $d = 5$ mm are shown in Fig. 2. The discharge is spontaneously ignited by a streamer-to-spark high-voltage transition but immediately after the breakdown the voltage drops to several hundred volts and a stable discharge was sustained. As seen in Fig. 2 the discharge current waveform oscillates with a frequency of 100 Hz, almost independent of the arc voltage evolution, because the discharge current is controlled by the transformer impedance. The voltage signal also has a frequency of 100 Hz, with large spikes at the beginning of each cycle (due to the quenching and re-ignition of the discharge).

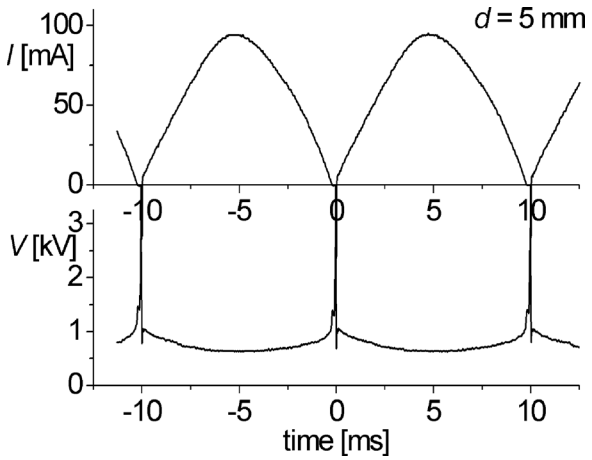

FIG. 2. Typical current and voltage waveforms of the discharge for $d = 5$ mm and 100 mA peak current.

Aside from the spikes, the voltage decreases (increases) when the current increases (decreases). This behavior results in a negative slope in the voltage-current characteristic of the discharge. A similar behavior was observed by other researches with intermediate-current discharges.[20,21]

The arc voltage as a function of the discharge length for different discharge currents is shown in Fig. 3. As it can be seen, for discharge lengths lower than 1 mm the curves are coincident (within the experimental uncertainty); indicating that for $d < 1$ mm the voltage becomes independent of the discharge current. The electric field strength (E) in the discharge, as given by the slope of the voltage-length curve, varies gently, reaching a constant value as the discharge length increases. This constant value is current-dependent, and varies from 75 ± 15 V/mm for 50 mA to 17 ± 3 V/mm for 200 mA. A good agreement exists between these inferred electric fields values and those published by others authors in high-pressure intermediate current discharges.[22]

The derived voltage-current characteristic curves for fixed discharge lengths are shown in Figs. 4 and 5. For $d = 400\ \mu$m a remarkable constant value of the discharge voltage of $V_C = 360 \pm 40$ V was measured for currents from 50 to 200 mA. This voltage drop value is in good agreement with the cathode fall measured by Machala *et al.*[12] in a similar discharge and also coincides with the published value for the normal cathode fall (370 V) in a low-pressure glow discharge in air with a copper cathode.[1]

For larger inter-electrode lengths, the discharge voltage falls as the current increases resulting in a negative slope in the voltage-current characteristic of the discharge. As an example, a characteristic curve for $d = 5$ mm (with the cathode fall value subtracted from the discharge voltage) is shown in Fig. 5.

B. Current density measurements

A well-defined discharge "fingerprint" which was usually circular and consisted of a central area of clean metal surrounded by a black ring was observed at the cathode surface after each discharge running. The diameter of the area

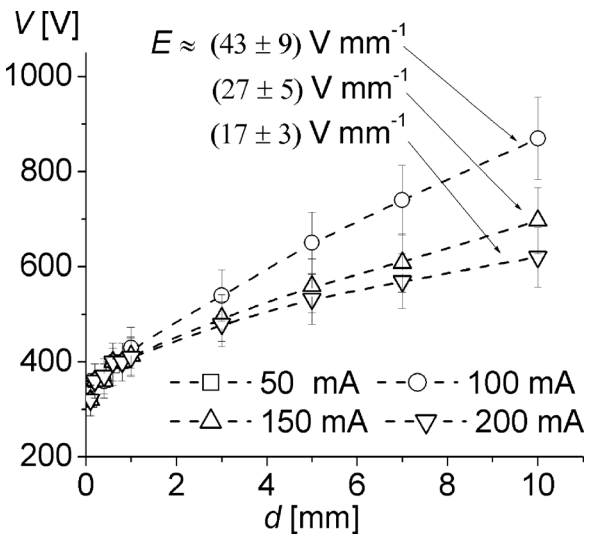

FIG. 3. Voltage-length curve of the discharge.

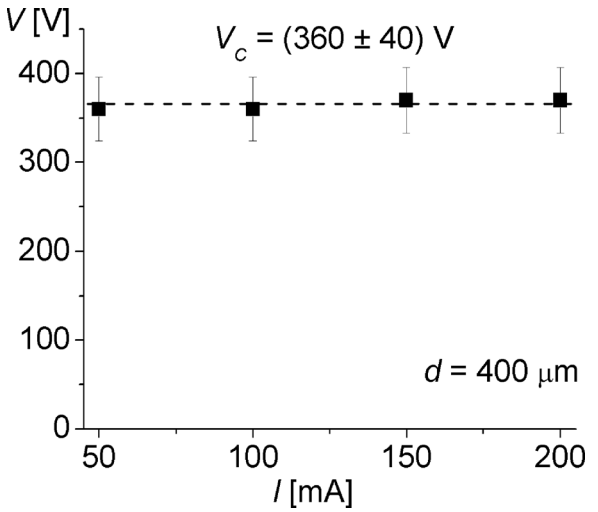

FIG. 4. Voltage-current characteristic curve for d = 400 μm.

of this clean copper "spot" was dependent on the discharge current, and was measured within an error of ± 0.1 mm. By assuming that the current flows in this region, the mean current density at the cathode surface was determined. Similar spots "fingerprint" were reported in an atmospheric pressure glow discharge in air with copper cathode.[22] The results of the measurements of the mean current density at the cathode are given in Fig. 6.

As it can be seen from Fig. 6, the "fingerprint" size of the discharge at the cathode surface depends linearly on the discharge current. This linearity indicates that the mean current density at the cathode is almost constant, as it is in the case of a normal glow discharge. The cathode current density (J_C) determined from the fit line slope (dashed line in Fig. 6) resulted 11 ± 1 A/cm^2. This value is larger than that corresponding to a normal glow but smaller than that of an arc. Similar values of the cathode current density were reported in high-pressure intermediate current glow discharges.[22]

For several different electrode spacing and discharge currents, discharge images were taken. For comparative

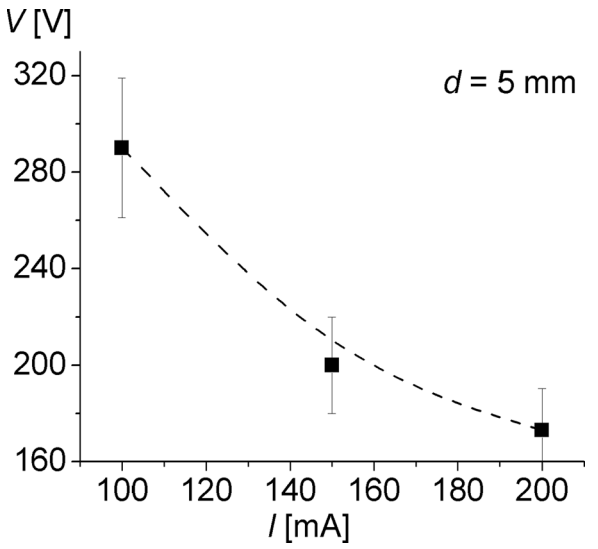

FIG. 5. Voltage-current characteristic curve for $d = 5$ mm.

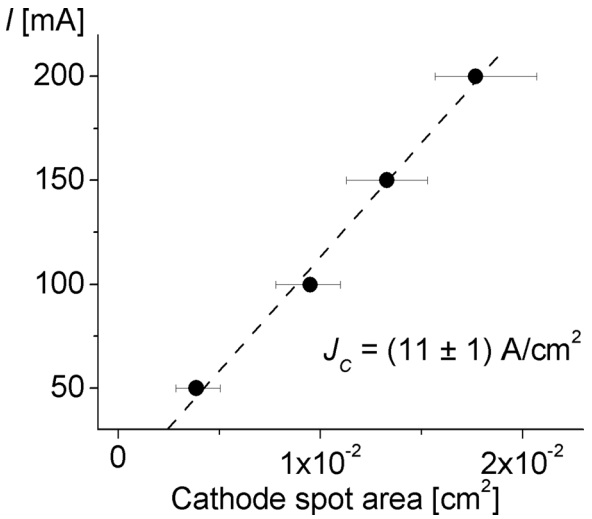

FIG. 6. Mean current density at the cathode.

purposes, all of the images were taken with an exposure time of 1/200 s (shorter exposure times where not possible because of poor camera sensitivity for the low-current discharges). According to the magnification of the employed optical system, the spatial resolution at the image plane was about 0.014 mm (70 pixels corresponded to 1 mm). A typical image for 100 and 150 mA and for $d = 1$ mm is shown in Fig. 7. The cathode (lower electrode) presents a large and bright spot, above which there is a dark space. After the dark space in the upper direction, there is a column which terminates at the anode in a small bright spot. Surrounding the column and the dark space there is a diffuse region with tenuous luminosity (the bright regions at the top and the bottom of the photographs are reflection of the discharge light on the electrodes). This visible pattern resembles the typical visible emissive structure of a low-pressure glow discharge;[1] thus suggesting a similar glow-like electric field distribution in the discharge. Gambling and Edels, operating at similar current levels,[22] registered also a diffuse region surrounding the column and the dark space. However, at lower currents (~1 to 10 mA) no surrounding diffuse region was observed.[15]

Images such as those shown in Fig. 7 were used to estimate the diameter of the current-carrying region of the discharge at the anode vicinities. As the time-scale of the discharge current (1/100 s) was of the order of the images exposure time (1/200 s); a large number of images (~100) were registered for every single discharge current and inter-electrode spacing. From this large group of images, only the brightest images that correspond to the passage of the discharge current by its peak value were selected and analyzed (having a similar pixel intensity distribution). It has been shown[23] that the diameter of the radiating region in low-current high-pressure discharges in air is about twice smaller than the size of the current-carrying region, due to strong dependence of the rate constant of excitation of the dominant N_2 radiating state on the reduced electric field. Hence, the diameter of the current-carrying region at the anode region of the discharge was defined as the width of the diffuse region around the central column. Employing the previously selected brightest image group (for every peak current value and inter-electrode spacing), the discharge widths were averaged. The resulting spreading error was about ±7 pixels (representing about ±0.1 mm). Using the discharge current peak value and the calculated area with the above described procedure, the mean current density of the discharge (J) was then calculated, and it is shown in Fig. 8 as a function of the peak discharge current.

As it can be seen from Fig. 8, for currents of 50 and 100 mA, the mean current density of the discharge at the anode side coincides (within the experimental uncertainty) with the value of the current density at the cathode. This is also true in low-pressure glow discharges if the discharge diameter is not greater than the discharge length.[1] The current-carrying diameter was 0.9 ± 0.1 and 1.2 ± 0.1 mm for 50 and 100 mA, respectively. For larger currents, the diameter of the current-carrying region remained constant (to a value of 1.2 ± 0.1 mm) and hence the current density increased linearly with the discharge current. These values are consistent with those that will be presented later obtained by determining the radius where the gas cooling (by radial thermal conduction) and electron impact heating of the gas balance each other.

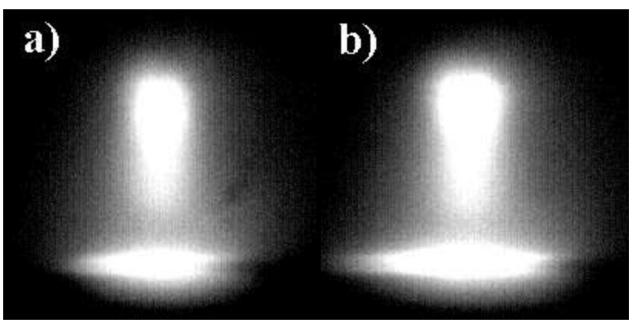

FIG. 7. Image of the discharge for $d = 1$ mm: (a) 100 mA, (b) 150 mA.

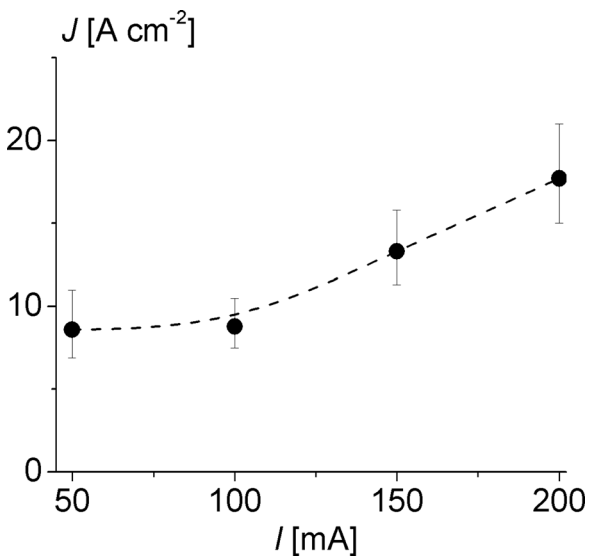

FIG. 8. Mean current density of the discharge at the anode region.

IV. KINETIC MODEL

In order to obtain an interpretation of the measurements, a numerical model of a stationary low-current discharge in atmospheric pressure air, taking into account non-equilibrium effects, was carried out.

The kinetic scheme was analogous to that developed in Refs. 23 and 24 for the simulation of low-current, atmospheric-pressure discharges in air. The included reactions are summarized in Table I. It included processes of electron-impact ionization (1), dissociative ionization (2), electron-ion recombination (3), electron attachment (4, 5), electron detachment (6–8), ion-ion recombination (9), electron-impact dissociation (10–11), ion conversion (12), and chemical reactions (13–22); including N_2, O_2, N, O, NO, NO^+, O^-, O_2^-, and O_3^- species and electrons. The used rate constants are given in $m^3\ s^{-1}$ for two-body processes and in $m^6\ s^{-1}$ for three-body processes, the temperatures T_g and T_e are given in K, and the reduced electric field E/n is in Td ($\equiv 10^{-21}$ V m^2).

The balance equations (evaluated in a local approximation)[24] were solved for the densities of N, O, NO, O^-, O_2^-, O_3^- and electrons. The density of positive ions was obtained from the condition of charge conservation, the density of N_2 was calculated by the condition of conservation of N and O nuclei (the air was assumed as the mixture N_2:O_2 = 4:1); and the density of O_2 was obtained from the condition that the total pressure was equal to the atmospheric one. The T_e and electron drift velocity (V_e) dependences on the reduced electric field were obtained by solving the Boltzmann kinetic equation with the help of the BOLSIG software package,[27] the corresponding cross sections being taken from Ref. 28. The plasma composition and the electron and gas temperatures were calculated from the condition that the discharge current density and the electric field values were equal to the experimentally inferred values. Note that the model output gives averaged values of the variables over the current-carrying area of the discharge.

V. RESULTS AND DISCUSSION

Since in atmospheric pressure discharges a noticeable difference between the vibrational temperature of the N_2 molecules and T_g takes place only at currents lower than 10 mA,[12,23,24] T_v was set equal to T_g during the calculations.

In Fig. 9, the obtained values of the electron and gas temperature of the discharge versus the discharge current are shown. A pronounced difference between the T_e and T_g

TABLE I. List of reactions.

Number j	Reaction	Rate constant k_j	Reference
1	$e + NO \rightarrow e + e + NO^+$	$5.0 \times 10^{-15} \exp[-460/(E/n)] \exp[6.5 \times 10^3 \exp[-3366/T_v]/(E/n)^2]$	24
2	$N + O \rightarrow e + NO^+$	$2.5 \times 10^{-23}\ T_g^{1.43} \exp[-31\,228/T_g]$	24
3	$NO^+ + e \rightarrow N + O$	$2.63 \times 10^{-15}\ T_g^{0.43} \exp[-31\,228/T_g]\ (T_g/T_e)^{1/2}\ (1-\exp[-2670/T_g])\ \exp[-75\,465/T_g]/\exp[-1.1\times10^5/T_g]$	24
4	$e + O_2 + O_2 \rightarrow O_2^- + O_2$	$4.2 \times 10^{-39}/T_e \exp[-604/T_g] \exp[697\ (T_e-T_g)/T_e/T_g]$	24
5	$e + O_2 \rightarrow O^- + O$	$6.7 \times 10^{-19} \exp[-1.05\|5.3-\ln(E/n)\|^3]\ (E/n)^{0.8} \exp[6.5\times10^3 \exp[-3366/T_v]/(E/n)^2]$	24
6	$O_2^- + O_2 \rightarrow e + O_2 + O_2$	$8.6 \times 10^{-16}\ (1-\exp[-1570/T_g])\ \exp[-6030/T_g]$	24
7	$O^- + O \rightarrow e + O_2$	5×10^{-16}	24
8	$O_3^- + O \rightarrow e + O_2 + O_2$	3×10^{-16}	24
9	$X^- + Y^+ \rightarrow X + Y$	$1.0 \times 10^{-8}/T_g^{1.5}$	24
10	$e + N_2 \rightarrow e + N + N$	$5.0 \times 10^{-15} \exp[-646/(E/n)] \exp[6.5 \times 10^3 \exp[-3366/T_v]/(E/n)^2]$	24
11	$e + O_2 \rightarrow e + O + O$	$1.7 \times 10^{-14} \exp[-324/(E/n)] \exp[6.5 \times 10^3 \exp[-3366/T_v]/(E/n)^2]$	24
12	$O^- + O_2 + M \rightarrow O_3^- + M$	$3.3 \times 10^{-40}/T_g$	25
	$M = N_2, O_2$		
13	$N_2 + M \rightarrow N + N + M$		
	$M = N_2, O_2, NO$	$5 \times 10^{-14} \exp[-113\,200/T_g]\ (1-\exp[-3354/T_g])$	26
	$M = O$	$1.1\times10^{-13} \exp[-113\,200/T_g]\ (1-\exp[-3354/T_g])$	26
14	$N + N + M \rightarrow N_2 + M$	$8.27\times10^{-46} \exp[500/T_g]$	26
15	$O_2 + M \rightarrow O + O + M$		
	$M = O_2$	$3.7\times10^{-14} \exp[-59\,380/T_g]\ (1-\exp[-2240/T_g])$	26
	$M = O$	$1.3\times10^{-13} \exp[-59\,380/T_g]\ (1-\exp[-2240/T_g])$	26
	$M = N_2, NO$	$9.3\times10^{-15} \exp[-59\,380/T_g]\ (1-\exp[-2240/T_g])$	26
16	$O + O + M \rightarrow O_2 + M$		
	$M = N_2$	$2.76\times10^{-46} \exp[720/T_g]$	26
	$M = O_2$	$2.45\times10^{-43}/T_g^{0.63}$	26
	$M = O$	$8.8\times10^{-43}/T_g^{0.63}$	26
17	$NO + M \rightarrow N + O + M$		
	$M = N_2, O_2$	$8.7\times10^{-15} \exp[-76\,000/T_g]$	26
	$M = O, NO$	$1.7\times10^{-13} \exp[-76\,000/T_g]$	26
18	$N + O + M \rightarrow NO + M$	$1.76\times10^{-43}/T_g^{0.5}$	26
19	$N + NO \rightarrow O + N_2$	$1.02\times10^{-18}\ T_g^{0.5}$	24
20	$O + N_2 \rightarrow N + NO$	$4\times10^{-18}\ T_g^{0.5}\ (1-\exp[-3367/T_g])\ \exp[-113778/T_g]/(1-\exp[-2670/T_g])/\exp[-75465/T_g]$	24
21	$N + O_2 \rightarrow O + NO$	$1.03\times10^{-20}\ T_g \exp[-3135/T_g]$	24
22	$O + NO \rightarrow N + O_2$	$2.1\times10^{-21}\ T_g \exp[-3135/T_g]\ (1-\exp[-2670/T_g])\ \exp[-75465/T_g])/\ (1-\exp[-2322/T_g])/\ \exp[-59211/T_g]$	24

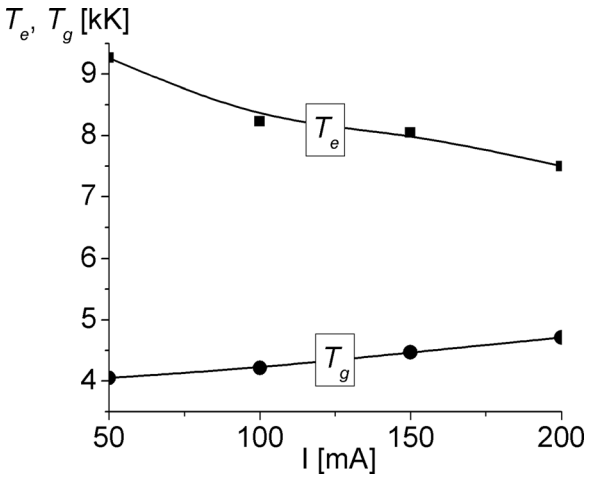

FIG. 9. Discharge electron and gas temperature versus the discharge current.

values is observed within the whole current range. As it can be seen, as the discharge current increases the electron temperature decreases, while the gas temperature increases (with rather high values, above 4000 K); consequently, the plasma non-equilibrium degree decreases. Both temperatures values show good agreement with published simulations of low-current, atmospheric-pressure discharges in air.[23,24] A rise in the gas temperature in air leads to the production of components such as NO, O, and N (shown in Fig. 10), which are usually absent in low-current glows. On the other hand, the reactions producing O, N, and NO are balanced by their inverse reactions (reactions (21) and (22) of Table I) in a sort of detailed balance. Since the rate constants in reactions (21)–(22) depend only on T_g, the densities of O, N, and NO reach equilibrium values which are determined by the gas temperature.

In Fig. 11, the number densities of the ions of the discharge versus the discharge current are shown. The presence of NO^+ ions is favored by the formation of NO because of its low ionization energy (=9.25 eV). The concentration of negative oxygen ions due to electron attachment is negligible as compared with those of NO^+ (and hence negligible as compared with the electron number density). This means

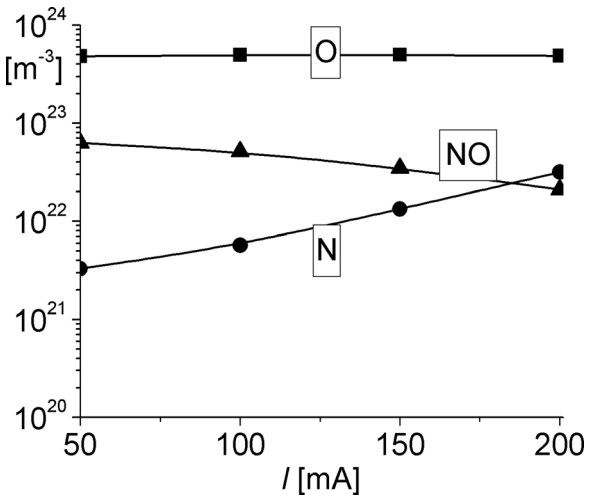

FIG. 10. O, N, and NO number densities versus the discharge current.

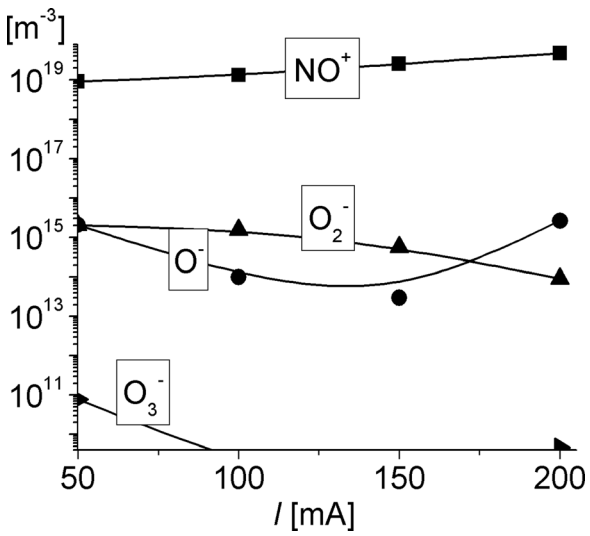

FIG. 11. Number densities of the ions of the discharge versus the discharge current.

that attachment does not play any significant role in this discharge.

Figure 12 shows the rates of electron production and loss via different mechanisms versus the discharge current. It is observed that the dominant process of production of electrons is the associative ionization as a consequence of the high gas temperature ($T_g > 4000$ K) within almost the whole current range. The production of electrons is determined by the value of the gas temperature and does not depend on the electron temperature. Note also that the ionization process is balanced by the reverse process (marked with a dashed line in Fig. 12), namely, dissociative recombination. With a decrease in the current (to values lower than 50 mA, not shown in Fig. 12) the reduced electric field increases, reaching a value at which the rate of ionization of gas particles by electron impact exceeds the rate of associative ionization.

The kinetic model shown that the discharge is mainly controlled by reactions (2) and (3) of Table I; that is, the

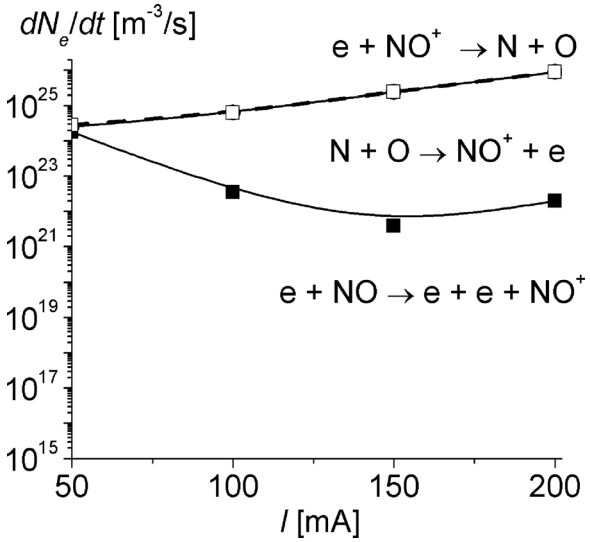

FIG. 12. Rates of electron production and loss via different mechanisms versus the discharge current.

value of the electron number density (N_e) can be determined from the simplified balance equation

$$k_2 N_O N_N = k_3 N_e^2, \quad (1)$$

(N_O and N_N are the number densities of O and N; respectively). It is significant that only k_3 depends on the electron temperature $T_e = T_e(E/n)$. As quoted before, under the considered conditions N_O and N_N are mainly controlled by the reactions (21) and (22) of Table I, which solely depend on T_g. Since k_2 is only a function of T_g as well, it follows from Eq. (1) that $k_3\ N_e^2$ must be independent of $T_e(E/n)$. Hence, the right hand side of Eq. (1) can be written as

$$k_3(T_e) N_e^2(T_e) = k_3(T_e = T_g) N_e^2(T_e = T_g), \quad (2)$$

where $N_e^2(T_e = T_g)$ is the local thermal equilibrium value of the electron number density in atmospheric pressure air. Then the electron density in the discharge can be estimated as

$$N_e(T_e) = \left(\frac{k_3(T_g)}{k_3(T_e)}\right)^{0.5} N_e(T_g). \quad (3)$$

Using Eq. (3), the current density in the discharge is given by

$$J = e V_e(E/n) \left(\frac{k_3(T_g)}{k_3(E/n)}\right)^{0.5} N_e(T_g). \quad (4)$$

Equation (4) allows the reduced field E/n to be calculated as a function of T_g and the experimentally inferred value of J for each current. The value of $N_e(T_e = T_g)$ for atmospheric-pressure air was obtained from Ref. 29. The results of this procedure are shown in Fig. 13.

As it can be seen from Fig. 13, a good agreement between the E/n values obtained from this simplified balance equation and from the experiment is achieved. The negative slope of the characteristic curve of the discharge can be understood because the value of the reduced electric field decreases as the discharge current increases since the associative ionization during collisions between O and N atoms dominates over electron-impact ionization (as a consequence of the high gas temperature, $T_g > 4000$ K).

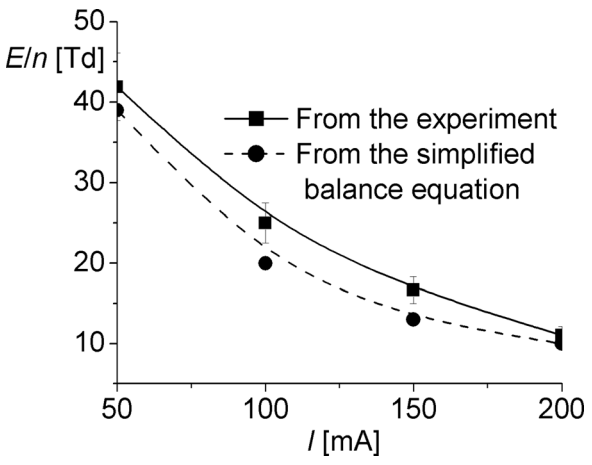

FIG. 13. Discharge reduced electric field versus the discharge current.

Low-current (~1 to 10 mA) atmospheric pressure glow discharges are stabilized by heat removal due to the neutral particles diffusion.[15,17] For higher currents, however, the neutral particles diffusion will be progressively replaced with heat conduction as T_g grows. To show this, consider the heat removal frequency due to neutral particles diffusion from a cylindrical volume of radius R: $\nu_D = D/\Lambda_D^2$ (where $\Lambda_D = R/2.4$ is the characteristic diffusion length and D is the diffusion coefficient, which is proportional to the mean-free-path and the molecular speed and thus has a $T_g^{3/2}/p$ dependence, being p the pressure).[1] For the same cylindrical volume, the heat removal frequency by thermal conduction is $\nu_T = \chi/\Lambda_T^2$ (where $\chi = \lambda/(nc_{pl})$ is the thermometric conductivity, being λ the thermal conductivity by heavy particles (including the reactive component), c_{pl} the specific heat at constant pressure per molecule and $\Lambda_T \approx R/2.8$ the averaged characteristic diffusion length).[1] The corresponding ratio $\nu_T/\nu_D \approx 1.4\lambda/(nc_{pl}D)$ varies from about 4 for $I = 50$ mA to about 20 for 200 mA, suggesting the progressively growing importance of heat conduction as I increases. In the quoted estimations, the heavy particles thermal conductivity for N_2 was obtained from Ref. 30, and the specific heat at constant pressure per molecule for high-temperature air was obtained from Ref. 2. D was taken as 1.47×10^{-5} m^2/s for N_2 in atmospheric pressure air.[15] Concerning the gas heating mechanism, the heating frequency for a single neutral is the electron–neutral heating collision frequency, which in turn is the electron density N_e times the rate constant for vibrational excitation of the neutral, k_{en}:$\nu_{heating} = N_e\ k_{en}$. For molecular gases like air the vibrational excitation of the molecule is the fastest mode of energy transfer between the electrons and neutrals.[15] By equating the heating and the thermal conduction cooling frequencies, an estimation for the radius of a stable discharge can be obtained. Calculations have been performed for discharges corresponding to four currents: 50, 100, 150, and 200 mA. The rate constants for vibrational excitation of N_2 were obtained from the BOLSIG code. The calculated radii for a stable discharge were 0.9, 1.5, 1.5, and 1.4 mm for 50, 100, 150, and 200 mA; respectively. Note that these values are rather close to the measured discharge radius: (0.9 ± 0.1) mm for 50 mA and (1.2 ± 0.1) mm for the larger currents. It can be seen that there is no simple correlation (neither experimental nor theoretical) between the discharge radius and the current value. A similar behavior for the discharge radius was reported in Ref. 24 through a numerical simulation of a similar low-current heat conduction-stabilized discharge. These results suggest that this discharge regime is stabilized by heat conduction.

The theoretical basis of the normal current density in low-pressure glow discharges states that the current density scale with pressure should only be a function of the discharge gas type, cathode material and gas pressure. This theory assumes that the gas is at room temperature (=293 K). For air and a copper cathode at room temperature, the normal current density scaling is $J_n/p^2 = 240\ \mu$A/cm^2/Torr^2.[1] However, for variable gas temperatures as high as 4000 K, the current density should be scaled with the gas

density (rather than the pressure); as $J_C = J_n\ p^2\ (293/T_g)^2$. The calculation of J_C for $T_g = 4000$ K gives 0.74 A/cm^2, which is one order of magnitude lower than the experimentally inferred value of the cathode current density ($= 11 \pm 1$ A/cm^2). However, it should be noted that the laws of similarity of the normal glow theory are only correct if the ionization processes in the discharge is controlled by direct electron impact[1] (which is true at low-gas temperatures in air); but not in this case due to the rather-high gas temperature (as shown Fig. 12).

VI. CONCLUSIONS

A Low-frequency (100 Hz), intermediate current (50 to 200 mA) glow discharge was experimentally investigated in atmospheric pressure air between copper blunt electrodes. A kinetic model for describing the ionization processes in the discharge was also carried out. The results have shown that:

(1) The visible emissive structure of the discharge resembles to that of a typical low-pressure glow thus suggesting a glow-like electric field distribution in the discharge.
(2) The discharge corresponds to a non-equilibrium plasma with rather high gas temperatures (above 4000 K).
(3) The high gas temperature leads to the production of components such as NO, O, and N (which are usually absent in low-current glows) which causes that the ionization by electron-impact will be replaced by associative ionization, being this last process independent of the reduced electric field. This leads to a negative current-voltage characteristic curve a priori unexpected for a common glow.
(4) Several estimations show that the discharge seems to be stabilized by heat conduction.

All the quoted results indicate that although this discharge regime might be considered to be close to an arc, it is still a glow discharge as demonstrated by its overall properties, supported also by the presence of thermal non-equilibrium.

ACKNOWLEDGMENTS

This work was supported by grants from the CONICET (PIP 11220090100219 and PIP 11220120100453) and Universidad Tecnológica Nacional (PID 1389 and PID 2264). L.P. and H.K. are members of the CONICET. J.C.C. thanks the CONICET for his doctoral fellowship. E.C. thanks the CIN for his under-graduate fellowship.

[1]P. Raizer, *Gas Discharge Physics* (Springer, Berlin, Germany, 1991).
[2]M. Boulos, P. Fauchais, and E. Pfender, *Thermal Plasmas, Fundamentals and Applications* (Plenum, New York, 1994), Vol. 1.
[3]V. A. Nemchinsky and W. S. Severance, J. Phys. D: Appl. Phys. **39**, R423 (2006).
[4]P. Fauchais, J. Phys. D: Appl. Phys. **37**, R86 (2004).
[5]A. Fridman, A. Chirokov, and A. Gutsol, J. Phys. D: Appl. Phys. **38**, R1 (2005).
[6]G. Faure and S. M. Shkol'nik, J. Phys. D: Appl. Phys. **31**, 1212 (1998).
[7]T. Verreycken, D. C. Schram, C. Leys, and P. Bruggeman, Plasma Sources Sci. Technol. **19**, 045004 (2010).
[8]D. B. Graves, Phys. Plasmas **21**, 080901 (2014).
[9]G. Y. Park, S. J. Park, M. Y. Choi, I. G. Koo, J. H. Byun, J. W. Hong, J. Y. Sim, G. J. Collins, and J. K. Lee, Plasma Sources Sci. Technol. **21**, 043001 (2012).
[10]Z. Machala, M. Janda, K. Hensel, I. Jedlovsky, L. Lestinska, V. Foltin, V. Martisovits, and M. Morvova, J. Mol. Spectrosc. **243**, 194 (2007).
[11]Yu. Akishev, O. Goossens, T. Callebaut, C. Leys, A. Napartovich, and N. Trushkin, J. Phys. D: Appl. Phys. **34**, 2875 (2001).
[12]Z. Machala, E. Marode, C. O. Laux, and C. H. Kruger, J. Adv. Oxid. Technol. **7**, 133 (2004).
[13]L. Yu, C. O. Laux, D. M. Packan, and C. H. Kruger, J. Appl. Phys. **91**, 2678 (2002).
[14]X. Lu, F. Leipold, and M. Laroussi, J. Phys. D: Appl. Phys. **36**, 2662 (2003).
[15]D. Staack, B. Farouk, A. Gutsol, and A. Fridman, Plasma Sources Sci. Technol. **14**, 700 (2005).
[16]V. I. Arkhipenko, A. A. Kirillov, L. V. Simonchik, and S. M. Zgirouski, Plasma Sources Sci. Technol. **14**, 757 (2005).
[17]D. Staack, B. Farouk, A. Gutsol, and A. Fridman, Plasma Sources Sci. Technol. **17**, 025013 (2008).
[18]A. Wilson, D. Staack, T. Farouk, A. Gutsol, A. Fridman, and B. Farouk, Plasma Sources Sci. Technol. **17**, 045001 (2008).
[19]S. Watanabe, S. Saito, K. Takahashi, and T. Onzawa, Weld. Int. **17**, 593 (2003).
[20]X. Li, X. Tao, and Y. Yin, IEEE Trans. Plasma Sci. **37**, 759 (2009).
[21]L. Giuliani, M. Xaubert, D. Grondona, F. Minotti, and H. Kelly, Phys. Plasmas **20**, 063505 (2013).
[22]W. A. Gambling and H. Edels, Br. J. Appl. Phys. **5**, 36 (1954).
[23]G. V. Naidis, Plasma Sources Sci. Technol. **16**, 297 (2007).
[24]M. S. Benilov and G. V. Naidis, J. Phys. D: Appl. Phys. **36**, 1834 (2003).
[25]I. A. Kossyi, A. Yu Kostinsky, A. A. Matveyev, and V. P. Silakov, Plasma Sources Sci. Technol. **1**, 207 (1992).
[26]N. L. Aleksandrov, E. M. Bazelyan, I. V. Kochetov, and N. A. Dyatko, J. Phys. D: Appl. Phys. **30**, 1616 (1997).
[27]See http://www.siglo-kinema.com/bolsig.htm for "CPAT & Kinema Software".
[28]A. V. Phelps and L. C. Pitchford, Phys. Rev. A **31**, 2932 (1985).
[29]A. Gleizes, J. J. Gonzalez, and P. Freton, J. Phys. D: Appl. Phys. **38**, R153 (2005).
[30]V. Nemchinsky, J. Phys. D: Appl. Phys. **38**, 3825 (2005).